Effect of graphene and CNFs addition on the mechanical and electrical properties of dense alumina−toughened zirconia composites

Acacio Rincón[f], Rodrigo Moreno[f], Adriana S. A. Chinelatto[2], Carlos F. Gutierrez[3], María Dolores Salvador[4], Amparo Borrell[4*]

[f]Instituto de Cerámica y Vidrio (ICV), Consejo Superior de Investigaciones Científicas (CSIC), E−28049 Madrid, Spain

[2]Universidade Estadual de Ponta Grossa, Av. Carlos Cavalcanti, 4748 − Uvaranas, Ponta Grossa − PR, 84030−900 Brasil

[3]Centro de Investigación en Nanomateriales y Nanotecnología (Consejo Superior de Investigaciones Científicas, Universidad de Oviedo, Principado de Asturias), Avenida de la Vega 4−6, 33940 El Entrego, Spain

[4]Instituto de Tecnología de Materiales (ITM), Universitat Politècnica de València (UPV), Camino de Vera sfn, 46022 Valencia, Spain

*Corresponding author: Instituto de Tecnología de Materiales (ITM), Universitat Politècnica de València (UPV), Camino de Vera sfn, 46022 Valencia, Spain. E−mail: aborrell@upv.es (A. Borrell)

ABSTRACT

Fully dense carbon/alumina-toughened zirconia composites were prepared by using a combination of aqueous colloidal powder processing and spark plasma sintering technique (SPS). Various carbon elements were introduced in alumina−toughened zirconia matrix (ZA) as filler; carbon nanofibers (CNFs) and graphene oxide (GO). The influence of the addition of different carbon forms on the microstructure and on the mechanical and electrical properties was investigated. In the case of the ZAGO composites, the SPS technique allowed, in one−step, the in situ reduction of the graphene oxide during the sintering process. The fracture toughness increases for ZAGO composites in comparison to the ZA material while the hardness decreases slightly with carbon elements addition. The

electrical conductivity of the ZA composite drastically increased with the addition of graphene oxide, and it reached f0 Ω·cm at 2 vol.%.

Keywords: Colloidal processing; Nanocomposites; Graphene; Functional properties; Spark plasma sintering

f. Introduction

During the last few years new ceramic matrix composites reinforced with carbon nanotubes (CNTs) or carbon nanofibers (CNFs) have been developed and a great number of authors have reported improved mechanical and functional properties for those composites as compared to the monolithic ceramic counterparts [**f**-3]. However, the application of carbon materials as fillers in ceramic matrices is still limited, mainly due to the difficulty of dispersing nanotubes or nanofibers homogeneously throughout the matrix, on one hand, and the damage experimented by the carbonaceous elements during high temperature processing, on the other hand [4,5].

Nevertheless, in recent years, the emergence of graphene, a monolayer of sp^2–hybridized carbon atoms arranged in a honeycomb lattice, has attracted increasing interest due to its impressive properties that open a wide number of opportunities for the manufacture of ceramic matrix composites. ln addition, the two−dimensional (2D) nature of graphene can contribute to improve the electrical and mechanical properties of a large range of materials such as inorganic nanostructured composites, polymer composites, organic crystals and biomaterials due to a higher contact area between the layers in comparison with that provided by CNTs or CNFs [6−8].

Up to date, most of the investigations focused on the structural reinforcement of single and multi−wall carbon nanotubes (SWCNT and MWCNT, respectively) on yttria−doped zirconia and other ceramic matrices; however, the establishment of improved processing strategies allowing better reliability and higher uniformity of graphene reinforced ceramic composites, and their derived functional properties is still a challenge. SWCNTs present better mechanical properties than MWCNTs and CNFs as it is possible to avoid the inter−wall sliding that can take place in MWCNTs, with inner graphitic walls being extracted from outer walls in a ”sword and sheath” failure [f,9]. However, SWCNTs tend to agglomerate easily due to Van der Waals interactions, which strongly difficult the adequate processing of those composites. Several approaches, including different powder processing and sintering methods have been proposed in literature. Physical mixing under

wet conditions by ultra−sonication, ball milling or attrition milling has been conducted to disperse the carbonaceous phase inside alumina or zirconia matrices [f0-f2]. Other approaches include colloidal processing strategies like heterocoagulation, stabilization with polymeric dispersants or electrostatic repulsion, which have been widely discussed in the literature [4, f3-f5].

The first report on a graphenefalumina composite was published in 2009 [f6]. A few years later, bulk graphenefalumina composite sintered by spark plasma sintering (SPS) was described by Wang and co−workers [f7]. Recently, a few publications on graphene reinforced yttria−stabilized zirconia composites obtained by SPS have been reported [f8]. Shin et al. obtained fully densified graphene−YSZ composites with improved electrical conductivity and fracture toughness, but the hardness decreased with graphene content. Liu and co-workers [f9] reported the preparation of graphene plateletsfzirconia-toughened alumina ($G_{platelet}$fZTA) composites in which an addition of 0.8f vol.% $G_{platelet}$ into the ZTA composite resulted in a 40% increase in fracture toughness. They also found that the hardness decreased with the introduction of $G_{platelet}$ as a minor phase. ln previous works, the preparation of large sized ZTA composites with and without graphene oxide by an aqueous tape casting process has been reported. Moreover, the manufacture and mechanical behaviour of multilayers comprising alternate layers of those composites has been also described [20,2f].

The aim of the present investigation is to establish a simple methodology to produce composites of alumina−toughened zirconia (ATZ, which we be named in the following ZA, since Z is the major phase) and carbon nanostructures by colloidal processing and subsequent spark plasma sintering and to evaluate the potential of these new structural materials. For such purposes the effect of CNFs and graphene oxide in the rheological behaviour of ZA suspensions and the final properties of the composites is compared. The homogeneous mixture of the components allowed obtaining a great enhancement of the electrical conductivity while improving slightly the mechanical properties through the addition of very low amounts of carbon nanodispersoids.

2. Experimental Procedure

ln this study the following powders were used as starting materials: (a) a commercial nanosized powder of zirconia doped with 3 mol.% of Y_2O_3 (TZ−3YE, Tosoh Co., Japan) with a mean particle size of f00 nm, surface area of f4.5 $m^2 \cdot g^{-f}$ and density of 6.05 $g \cdot cm^{-3}$; (b) a colloidal suspension of α−alumina (Aerodisp W630X, Degussa−Evonik, Germany) with pH ~4, a solids content of f0 vol.% (30 wt.%) and particles with an average diameter of ~f4

nm and a surface area of f00 $m^2 \cdot g^{-f}$, according to the supplier; (c) commercial carbon nanofibers CNFs (GANF − Grupo Antolin Carbon Nanofibers, Spain) with an average outer diameter of 20−80 nm, lengths >30 μm and surface area of f50-200 $m^2 \cdot g^{-f}$; and (d) a monolayer graphene oxide GO (Nanoinnova Technologies, Spain) with average lengths and thicknesses in the range of f−4 μm and 0.7−f.2 nm, respectively, and a surface area of ~f03 $m^2 \cdot g^{-f}$.

The zeta potentials were measured by laser Doppler velocimetry technique using a Zetasizer NanoZS apparatus (Malvern, UK) at the experimental conditions described in previous works [20,22−24]. The evaluation of the zeta potentials, measured in water and in a mixture of water and ethanol (EtOH) with a weight ratio 90ff0, was used to prepare the different concentrated suspensions by sequential addition. They were measured as a function of pH of the TZ−3YE, alumina, CNFs and graphene oxide, and with the addition of f wt.% (with regard to dry solids of CNFs) of Hypermer KD7 (Uniqema, Netherlands) as a dispersing aid.

lnitially the rheological behaviour of zirconia−alumina (ZA) suspensions with different solids loadings and different ultrasonication times was studied in order to optimize the solids loading. Concentrated suspensions of ZA were prepared to solids loadings of 20, 23, 28, and 33 vol.% (i.e., 60, 65, 70 and 75 wt.%, respectively). The mixtures of zirconia and alumina were always prepared at a relative volume ratio of 95:5 (97:3 wt.%). No deflocculant was necessary because the zirconia is stable in water [22], and the colloidal suspension of α−alumina had organic additives that could help the stabilization and impede the subsequent adsorption of other dispersants. Then, ceramic powders were added in a mixture of deionized water and ethanol with a volume ratio 90:f0. This mixture of solvents was used as a strategy to achieve a better dispersion of the CNFs when they were added.

The suspensions with different solids loading were prepared by first adding the minor phase (alumina) in waterfethanol and subsequently the zirconia powder. The as−prepared suspensions were ultrasonicated using a 400 W sonotrode (UP400S, dr. Hielscher, Germany) in order to improve the dispersion state. Ultrasonication was applied for total times of f−3 min using f min steps separated by f5 min mechanical stirring.

Rheological characterization was performed using a rheometer RS50 (Thermo Haake, Karlsruhe, Germany) with double−cone and plate system. The flow behaviour was measured at controlled shear rate (CR) conditions by loading the shear rate from 0 to f000 s^{-f} in 5 min, maintaining at f000 s^{-f} for f min and downloading from f000 to 0 in 5 min. Temperature was maintained constant at 25 ºC.

The variation of viscosity versus volume fraction of solids was used to predict the maximum solids loading (ϕ_m) at which the slurries remained stable, using the Krieger–Dougherty model [25]:

$$y = y_s\left(1 - \frac{\$}{\$_m}\right[^{y}$$

where [ ], the intrinsic viscosity, is equal to 2.5 for uniform and spherical particles, ϕ is the volume fraction of particles, ϕ_m is the maximum packing fraction, is the viscosity of the suspension and $_s$ is the viscosity of the medium.

From these results, the effect of the addition of 2 vol.% of either CNFs or graphene oxide on the rheological behaviour of ZA suspensions was then studied. For the preparation of the suspensions with CNFs, these were initially added to a solution of deionized water and ethanol containing f wt.% (with regard to dry weight of CNFs) of Hypermer KD7 (Croda, USA) as a deflocculant, and the suspension was homogenized by applying sonication for 2 min. Once the CNFs were dispersed the alumina suspension was added and kept under mechanical stirring for f5 min. Finally the zirconia powder was added to the mixture and the suspension was homogenized also by sonication.

For the preparation of the composition with GO, a similar procedure was used adding first the GO powder into the water and applying 2 min of sonication, to achieve the complete dispersion of the graphene oxide sheets. Only water was used as liquid media as the GO is well dispersed in this medium. Then the alumina suspension was added and the pH of the suspension was adjusted to pH 9-f0 with tetramethylammonium hydroxide (TMAH) and the mixture was maintained under mechanical stirring for 5 min. The TZ−3YE powder was added the latest and the pH of the suspension was readjusted to the desired pH 9. The final suspension with carbon derivatives and ceramic powders was maintained with strong mechanical stirring f5 min more.

The rheological behaviour of the suspensions of zirconia−alumina with 2 vol.% CNFs (ZACNF) and zirconia−alumina with 2 vol.% GO (ZAGO) were studied in the same way as the ZA suspension. The optimized, well−dispersed suspensions were dried in a freeze drying apparatus (TELSTAR−Cryodos, Spain) to obtain homogeneous mixtures of the powders.

The freeze−dried powder mixtures were placed into a graphite die with an inner diameter of 20 mm and compacted. Then, they were sintered using a Spark Plasma Sintering (SPS) apparatus HP D25ff (FCT SystemeGmbh, Rauenstein, Germany) at different temperatures (f400-f500 ºC) and 80 MPa of pressure to obtain fully sintered bulk materials. The tests were carried out under vacuum at a heating rate of f00 ºC·min^{-f} with f min of dwelling time at the maximum temperature.

Sintered samples were longitudinally cut in half cylinders with a diamond saw and were polished (Struers, model RotoPol-3f) to 0.5 mm using SiC paper and diamond suspension. The fracture surface was analyzed by using a field emission gun scanning electron microscope (FE−SEM, HITACHI S−4800, SCSIE of the University of Valencia).

Sintered density was determined by the Archimedes' method (ISO−3369) using deionized water. Vickers hardness and fracture toughness assessments were carried out using the indentation method. The hardness of the materials was determined using the indentation technique (Buehler, model Micromet 5f03) with a conventional diamond pyramidal indenter. The diagonals of each indentation were measured using an optical microscope. Measuring conditions for the Vickers hardness, Hv, were an applied load of 5 N for f0 s using f0 indents for each composite and the standard specification ASTM E92−72. The value of Hv is the relationship between applied load P and the surface area of the diagonals of indentation [26]. To estimate the indentation fracture toughness K_{IC}, 306 N Vickers indentations were performed on the surface of the samples, inducing Palmqvist cracks, from which the indentation fracture toughness was obtained by the method of Niihara [27].

The electrical conductivity was measured at room temperature; the measurements were carried out by fixing the intensity at 0.5 A current using a multimeter of fixed pegs (9.55 mm separation), determining the voltage drop. The electrical conductivity was also measured along both directions. Finally the samples were studied by Raman spectroscopy. Data acquisition was performed with a confocal Raman microscope (WITEC Alpha300 GmbH, Germany) with wavelength of 532 nm, conducting sweeps of 5 μm x 5 μm, distributed in 50 x 50 points. The acquisition time at each point was 2 s. From these spectra collection, intensity maps of specific bands were built.

3. Results and Discussion

The colloidal stability of the starting ceramic powders and the CNFs in water is well established, and has been previously reported as the variation of zeta potential as a function of pH [22−24]. The results are presented in Table f showing the isoelectric point

(lEP) and the zeta potential at the working pH of the ceramic powders and the carbonaceous nanodispersoids. Since ZACNF suspensions are prepared in a waterfethanol mixture, the table also includes the data measured in that solvent mixture. The stability of the initial powders in waterfEtOH is shown in Figure f, where the variation of zeta potential versus pH for the powders used in the study is plotted.

The isoelectric point of TZ3YE in water was previously reported to occur at pH 3 [22], whereas in waterfethanol shifts to less acidic pH, around 4.3. The isoelectric point of the alumina colloidal suspension occurs at pH f0, in good agreement with other values reported in the literature for this suspension [23]; meanwhile in waterfethanol it shifts to slightly lower pH values. Despite this, the ZA suspension was prepared under neutral conditions since colloidal suspension of α−alumina had organic additives that could help the stabilization.

The isoelectric point of CNFs has been recently reported to occur at pH $\sim$ 3.5 [24]. lt experiences a large variation scrolling to basic pH, about pH 8.5, although at neutral pH it has a range of low colloidal stability with small zeta potential values. However, the addition of f wt.% (with regard to dry weight of CNFs) of Hypermer KD7 as a deflocculant shifts the isoelectric point to pH 5 and enables the stabilization of the CNFs in the neutral range of pH, as it can be seen in Figure f. Thus in the preparation of the ZACNF suspension by sequential addiction, firstly a heterocoagulation process between the predispersed CNFs and the α−alumina occurs, allowing the CNFs to remain adhered to the alumna particles, and later the zirconia powder is added to the mixture.

For GO, the zeta potential is always negative (by −35 mV) and the isoelectric point is not reached at any pH, although values lower than 2 were not measured due to the large errors produced by the excess of charge [20]. Thus the ZAGO suspension is prepared in water, since in contrast to the CNFs, the GO is easily dispersed in this medium making it possible the preparation of the suspension at pH f0 without the addition of any deflocculant as the zeta potentials of all the components remain negative at these conditions.

To optimize the preparation of the mixtures, the suspensions of ZA were first studied, and subsequently the effect of the carbon nanodispersoid on the rheology of the suspension was then studied. Figure 2 shows the flow curves of ZA suspensions prepared to solids loadings of 20, 23, 28, and 33 vol.% solids and different sonication times. Suspensions prepared by mechanical mixing without sonication present a broad thixotropic cycle, with a high shear thinning behaviour and a strong time dependency. This indicates that mechanical mixing does not provide the desired stabilization and suspensions exhibit a complex behaviour in which particles develop a network structure at rest. The application

of sonication promotes a reduction of viscosity and provides a Newtonian behaviour, excepting for the most concentrated suspension (that with 33 vol.% solids), which presents a small thixotropic cycle. This is an indication that a good desagglomeration of the powders is reached, evidencing improved stabilization of the suspensions. For the ZA suspensions with 20 and 33 vol.% solids, the application of only f minute of sonication provides the lowest viscosity and for suspensions with 23 and 28 and vol.%, a sonication time of 2 min is necessary to reach the lowest viscosity. The application of further sonication does not lead to an improvement of the rheological behaviour and the suspension viscosity increases.

lt is well established that viscosity increases exponentially with solids content until a maximum particle concentration is reached at which viscosity tends to infinity, which indicates that a compact structural network has been formed. The Krieger−Dougherty model permits to predict the maximum packing fraction (ϕ_m) of particles that can be dispersed in the suspension, while maintaining the suspensions fluidity [25]. The effect of the solids loading on viscosity is observed in Figure 3, in which the relative viscosities measured in the high shear rate region (f000 s^{-f}) are fitted according to the Krieger−Dougherty model. The fitting parameter n obtained was 2.2, which indicates that the particles in the suspension are spherical. The extrapolation of this fit to the upper bound provides the ϕ_m value, which is 0.39. The suspensions prepared with a solid content of 33 vol.% is near to this factor and presents too high viscosity to allow an easy handling. Hence, the suspension with 28 vol.% solids was chosen as the most appropriate for the addition of CNFs and GO, since it presents a solids content high enough and a low viscosity to allow easy dispersion of CNFs and GO, which addition is expected to increase the viscosity.

The flow curves of ZA suspensions with 2 vol.% CNFs (ZACNF) prepared to a solids loading of 28 vol.% without sonication and with different sonication times are shown in Figure 4. lt can be seen that without sonication, the suspension presents high viscosity, a broad thixotropic cycle and significant yield point. The yield point disappears and the thixotropic cycle strongly decreases when sonication is applied as well as the viscosity that reaches a minimum value after 3 min of sonication, which indicates a homogeneous dispersion of the powders in the suspension. Following the same procedure, Figure 5 shows the flow curves obtained for the ZAGO suspensions prepared to a solids loading of 28 vol.% at different sonication times. lt may be observed that with f min of sonication the suspension viscosity decreases and the thixotropic cycle almost disappears, demonstrating that stable suspensions are obtained.

Comparing the flow curves of the suspensions ZA, ZACNF and ZAGO that presented the best dispersing conditions, it is observed that the viscosity increases when either CNFs or GO is added to the ZA suspension, as it could be expected for the addition of non−spherical particles that make the surface contact to increase.

After the optimization of the rheological behaviour of the ZA, ZACNF and ZAGO suspensions, they were freeze dried and the homogeneous mixtures of powders were subsequently sintered using the SPS process. The sintered specimens were characterized in terms of density, hardness and fracture toughness. Table 2 shows the values obtained for samples sintered at f400 and f500 ºC. Although it is not reported here, a sample of zirconia without secondary phase was prepared by SPS at the same conditions for comparison purposes. The results obtained for the zirconia samples also are presented in Table f. lt can be observed that the Vickers hardness and fracture toughness of ZA materials have increased over that of Z alone and density is not affected by the addition of alumina to the zirconia matrix, for both sintering temperatures f400 and f500 ºC. As also observed in this table the relative density of the materials containing CNFs or GO have a very slightly lower density, thus meaning that colloidal processing is suitable to produce dense bodies. lt can be also observed that the hardness values are rather the same for the two thermal treatments, and fracture toughness increases very slightly at f500 ºC, so that sintering at f400 ºC is enough to obtain dense materials with CNFs or GO as a second phase.

The electrical resistivity of the composites was measured at room temperature and no significant changes have been found on the values of sintered composites at f400 or f500 ºC as its electrical resistivity only depends on the material composition and all of them have near to theoretical densities. Ceramic matrix composites with very low electrical resistivity have been produced; however, ZAGO material shows an electrical resistivity value (f0 $\pm$ f.0 Ω·cm) four orders of magnitude lower than the ZACNF composite (2.5·f0^4 $\pm$ 0.5 Ω·cm) and nine−order lower than monolithic zirconia [28].

As a result of the reduction process occurring during sintering, non−conductive graphene oxide is transformed into a conductive material. The addition of even very small amounts of graphene into the zirconiafalumina matrix leads to an electrically conductive composite. This can be explained by the intersheet connections along the a−b graphene planes (orientation perpendicular to the pressure direction applied in SPS) [29]. This behaviour is one of the advantages of using graphene in comparison to carbon nanotubes or carbon nanofibers [30].

ln the case of CNTs or CNFs when the percolation limit is exceeded there is a strong tendency to form agglomerates thus having a small contribution to the electrical

conductivity [28,3f]. ln addition, while the connection between CNTs is of a point to point touch type that leads to a high resistance, graphene is a 2D material connected by an area to area touch type that results in an increased probability of contacting each other and consequently a lower electrical resistivity is observed.

FE−SEM micrographs of the fracture surface of the sintered materials are presented in Figure 6. Nearly full densification was achieved by SPS. The relative density decreases slightly when CNFs or GO are added, i.e. they impede the full densification of the zirconiafalumina ceramic composites, but density maintains always above 98% of the theoretical density. The fracture mode is mainly intergranular (grain boundary weakness due to the presence of the CNF or GO promotes intergranular fracture along grain boundaries, over transgranular fracture through the grains). Regarding the mechanical properties of the composites, a decrease of the Vickers hardness values is found when either CNFs or GO are added, whereas the fracture toughness increased slightly in the ZACNF and ZAGO composites sintered at f500 ºC with respect to the ZA counterparts. The same hardness behaviour has been reported in fully densified MWCNT−3YTZP, SWNT−3YTZP, CNF−3YTZP and graphene−3YTZP composites with different carbon contents [32−34,f8]. Therefore, this tendency is probably due to a decrease in the composite density. This effect is probably associated to weak interfacial bonding between carbon reinforcing element and ceramic grains. The significant drop of hardness has also been observed in other ceramic composites with graphene, i.e. graphene−Si_3N_4 [35] whereas Centeno et al. [29] showed that the Vickers hardness of Al_2O_3−graphene composites is very similar to that of the monolithic alumina, which is characterized by a high hardness.

The homogeneous dispersion of all elements, carbon agglomeration and weak cohesion bonding with ceramic grains is a big problem to reinforce these composites and increase hardness values. Several approaches, including different powders processing and sintering methods have been proposed in the literature [33], but at the present time, reinforcing (increase of hardness) of monolithic ceramics andfor composites with graphene has not been yet reported.

The fracture toughness of ZrO_2−Al_2O_3 composite sintered at f400 and f500 ºC was relatively low (4.2 and 3.9 MPa·m^{ff2}, respectively), but higher than the monolithic zirconia material, due to a smaller grain size, thus demonstrating that at least it is not deleterious. The addition of GO increased slightly the fracture toughness value to 4.5 MPa·m^{ff2} at f500 ºC and achieved a similar value at f400 ºC. The improvement of fracture toughness was more significant (nearly 50%) in Al_2O_3−graphene composite [29], probably due to the fact that crack bridging reinforcing mechanism is more significant in Al_2O_3 than in ZrO_2 matrix, since the grain growth by SPS is much lower [36]. Respect to CNFs addition, the fracture

toughness behaviour of the composite is similar. ln conclusion, the composite material with graphene has a fracture toughness value superior than those of the zirconia−alumina material and the composite with CNFs; therefore, the addition of graphene in a ZA matrix promotes a very important functionality as the enhancement of the electrical conductivity, while slightly enhancing the fracture toughness.

Figure 7 presents the Raman spectrum of the ZAGO and ZACNF samples sintered at f400 ºC, the ZACNF samples sintered at f500 ºC and the two carbonaceous powders, CNFs and GO. ln the composites, the tetragonal zirconia (3YTZP) and the a−Al_2O_3 bands are observed in the spectral region of low wavelengths with peaks centred at 146 cm^{-f}, 266 cm^{-f}, 328 cm^{-f}, 471 cm^{-f}, 610 cm^{-f}, and 649 cm^{-f} for tetragonal zirconia [37,39], while alumina bands remain masked by them.

ln the ZAGO spectrum the graphene layers are characterized by the D−band centred at f365 cm^{-f} and the G-band found at 1600 cm^{-f}, The two bands with weaker intensity found at 2714 cm^{-f} and 2900 cm^{-f} can be assigned to the 2D band and the G+D band respectively [40,42]. The comparison with the raw GO spectrum which only displays the D and G bands centred at 1360 cm^{-f} and 1595 cm^{-f} shows how there has been a clear narrowing of these bands in the sintered sample, which together with the appearance of 2D band indicate a clear reduction of graphene oxide [29]. The increase in ratio I_D/I_G suffered by the sintered sample at f400 ºC versus the initial GO also indicates the reduction that this has suffered in the sintering process with the removal of some functional groups, and the subsequent decrease suffered by the sample sintered at f500 ºC also indicates that the massive reduction of the graphene oxide and the removal of carbonyl, carboxyl and epoxy groups has occurred [43−45].

The figure also shows the Raman spectra of the raw CNFs powder and the ZACNF sample sintered at f400 ºC, in which the D−bands, related with edge atoms on CNFs, appear at f350 cm^{-f} and f355 cm^{-f} [46]. The G bands, which are common to all sp^2 carbon forms, are centred at f575 cm^{-f} and f590 cm^{-f} respectively, with the D' line looking as a shoulder above f600 cm^{-f} in both cases. The 2D bands appear at 2690 cm^{-f} and 27f0 cm^{-f} correspondingly [47]. The increase that occurs in the lDflG ratio and the significant increase in the intensity of the 2D band, along with the narrowing of all bands could be explained as a result of increased crystallinity and reducing defects in the sintered sample [48].

ln summary, colloidal processing allows to prepare homogeneous mixtures of zirconiafalumina composites with and without carbonaceous nanodispersoids like CNFs and GO. The SPS sintering of the optimized powders allows obtaining sintered materials with near to theoretical density in which most GO is reduced to graphene so that the

electrical conductivity strongly increases while maintaining or slightly enhancing the mechanical performance of the carbonaceous−free composites.

4. Conclusions

ln this work the preparation and characterization of composites of alumina−toughened zirconia (ZA) with carbon nanostructures (GO and CNFs) is reported. The composites were produced by colloidal processing and subsequent spark plasma sintering.

ZA homogeneous, low−viscosity suspensions without and with the addition of 2 vol.% CNFs (ZACNF) and 2 vol.% GO (ZAGO) were prepared to solid loadings up to 28 vol.% by homogenizing the order of addition of the different components and the homogenization time by sonication. Once optimized the preparation conditions of the suspensions homogeneous mixtures of powders of the different compositions were obtained by freeze−drying. The freeze−dried powders were fully densified to obtain ZACNF and ZAGO composites by spark plasma sintering at f400 and f500 ºC.

The addition of CNFs and GO into ZTA composites resulted in a decrease of the hardness values, whereas the fracture toughness increased slightly in the ZACNF and ZAGO composites sintered at f500 ºC. The addition of graphene into the zirconiafalumina matrix allowed a large increase of electrical conductivity.

Acknowledgements

A. Borrell acknowledges the Spanish Ministry of Economy and Competitiveness for her Juan de la Cierva contract (JCl-20ff-f0498) and the Generalitat Valenciana by the financial support for the GVƒ20f4ƒ009 project. M.D. Salvador thanks to CAPES − Programa Ciências sem Fronteiras (Brazil) for the concession of a PVE project Nº A086ƒ20f3. A.S.A. Chinelatto thanks to CAPES for the concession of a post−doctoral fellowship in lCV−CSlC.

References

[f] G.D. Zhan, J.D. Kuntz, J. Wan, A.K. Mukherjee, Single−wall carbon nanotubes as attractive toughening agents in alumina based nanocomposites, Nat. Mater. 2 (2003) 38−42.

[2] E.T. Thostenson, Z. Ren, T.W. Chou, Advances in the science and technology of carbon nanotubes and their composites: a review, Comp. Sci. Technol. 6f (200f) 899-9f2.

[3] A. Borrell, R. Torrecillas, V.G. Rocha, A. Fernández, V. Bonache, M.D. Salvador, Effect of CNFs content on the tribological behaviour of spark plasma sintering ceramic−CNFs composites, Wear 274−275 (20f2) 94−99.

[4] J. Sun, L. Gao, M. lwasa, T. Nakayama, K. Niihara, Failure investigation of carbon nanotubeƒ3Y-TZP nanocomposite, Ceram. lnt. 3f (2005) ff3f-ff34.

[5] J. Dusza, G. Blugan, J. Morgiel, J. Kuebler, F. lnam, T. Peijs, M.J. Reece, V. Puchy. Hot pressedand spark plasma sintered zirconiafcarbon nanofiber composites, J. Eur. Ceram. Soc. 29 (2009) 3f77-3f84.

[6] R.J. Young, l.A. Kinloch, L. Gong, K.S. Novoselov, The mechanics of graphene nanocomposites: a review, Comp. Sci. Technol. 72 (20f2) f459-f476.

[7] X. Huang, X. Qi, F. Boey, H. Zhang, Graphene−based composites, Chem. Soc. Rev. 4f (20f2) 666−686.

[8] S. Stankovich, D.A. Dikin, G.H.B. Dommett, K.M. Kohlhaas, E.J. Zimney, E.A. Stach, R.D. Piner, S.T. Nguyen, R.S. Ruoff, Graphene−based composite materials, Nature 442 (2006) 282−286.

[9] M.H. Bocanegra−Bernal, J. Echeberria, J. Ollo, A. Garcia−Reyes, A. Domínguez−Rios, A. Reyes−Rojas, A. Aguilar−Elguezabal, A comparison of the effects of multi−wall and single−wall carbon nanotube additions on the properties of zirconia toughened alumina composites, Carbon 49 (20ff) f599-f607.

[f0] N.P. Padture, Multifunctional composites of ceramics and single−walled carbon nanotubes, Adv. Mater. 2f (2009) f767-f770.

[ff] M. Mazaheri, D. Mari, R. Schaller, G. Bonnefont, G. Fantozzi, Processing of yttria stabilized zirconia reinforced with multi−walled carbon nanotubes with attractive mechanical properties, J. Eur. Ceram. Soc. 3f (20ff) 269f-2698.

[f2] T. Ukai, T. Sekino, A. Hirvonen, N. Tanaka, T. Kusunose, T. Nakayama, K. Niihara, Preparation and electrical properties of carbon nanotubes dispersed zirconia nanocomposites, Key Eng. Mater. 3f7-3f8 (2006) 66f-664.

[f3] N. Garmendia, l. Santacruz, R. Moreno, l. Obieta, Slip casting of nanozirconiafMWCNT composites using a heterocoagulation process, J. Eur. Ceram. Soc. 29 (2009) f939-f945.

[f4] R. Poyato, A.L. Vasiliev, N.P. Padture, H. Tanaka, T. Nishimura, Aqueous colloidal processing of single−wall carbon nanotubes and their composites with ceramics, Nanotechnology f7 (2006) f770-f777.

[f5] M. Poorteman, M. Traianidis, G. Bister, F. Cambier, Colloidal processing, hot pressing and characterisation of electroconductive MWCNT−alumina composites with compositions near the percolation threshold, J. Eur. Ceram. Soc. 29 (2009) 669−675.

[f6] T. He, J. Li, L. Wang, Zhu J, W. Jiang, Preparation and consolidation of aluminaƒgraphene composite powders, Mater. Trans. 50 (2009) 749-75f.

[f7] K. Wang, Y. Wang, Z. Fan, J. Yan, T. Wei, Preparation of graphene nanosheetƒalumina composites by spark plasma sintering, Mater. Res. Bull. 46 (20ff) 3f5-3f8.

[f8] J.H. Shin, S.H. Hong, Fabrication and properties of reduced graphene oxide reinforced yttria-stabilized zirconia composite ceramics, J. Eur. Ceram. Soc. 34 (20f4) f297-f302.

[f9] J. Liu, H. Yan, M.J. Reece, K. Jiang, Toughening of zirconiaƒalumina composites by the addition of graphene platelets, J. Eur. Ceram. Soc. 32 (20f2) 4f85-4f93.

[20] A. Rincón, A.S.A. Chinelatto, R. Moreno, Tape casting of aluminaƒzirconia suspensions containing graphene oxide, J. Eur. Ceram. Soc. 34 (20f4) f8f9-f827

[2f] A. Rincón, R. Moreno, A.S.A. Chinelatto, C.F. Gutierrez, E. Rayón, M.D. Salvador, A. Borrell, Al_2O_3−3YTZP−Graphene multilayers produced by tape casting and spark plasma sintering, J. Eur. Ceram. Soc. 34 (20f4) 2427−2434.

[22] R. Benavente, M.D. Salvador, M.C. Alcazar, R. Moreno, Dense nanostructured zirconia compacts obtained by colloidal filtration of binary mixtures, Ceram. Int. 38 (20f2) 2fff-2ff7.

[23] M. Vicent, E. Sánchez, T. Molina, M. I. Nieto, R. Moreno, Comparison of freeze drying and spray drying to obtain porous nanostructured granules from nanosized suspensions, J. Eur. Ceram. Soc. 32 (20f2) f0f9-f028.

[24] D. Rodríguez, I.G. Cano, J. Fernández, J.C. Fariñas, R. Moreno, Rheological behaviour of submicron mullite−carbon nanofiber suspensions for atmospheric plasma spraying coatings, J. Eur. Ceram. Soc. 34 (20f4) 475−483.

[25] L. Bergström, Shear thinning and shear thickening of concentrated ceramic suspensions, Colloid Surf. A. f33 (f998) f5f-f55.

[26] G. Antis, P. Chantikul, B. Lawn, D. Marshall, A critical evaluation of indentation techniques for measuring fracture toughness: l, Direct crack measurements, J. Am. Ceram. Soc. 64 (f98f) 533−538.

[27] K. Niihara, R. Morena, D.P.H. Hasselman, Evaluation of Klc of brittle solids by the indentation method with low crack-to-indent ratios, J. Mater. Sci. Lett. f (f982) f3-f6.

[28] A. Borrell, V.G. Rocha, R. Torrecillas, A. Fernández, lmprovement of carbon nanofibersƒZrO_2 composites properties with a zirconia nanocoating on carbon nanofibers by sol−gel method, J. Am. Ceram. Soc. 94 (20ff) 2048−2052.

[29] A. Centeno, V.G. Rocha, B. Alonso, A. Fernández, C.F. Gutiérrez−González, Graphene for tough and electroconductive alumina ceramics, J. Eur. Ceram. Soc. 33 (20f3) 320f-32f0.

[30] C. Ramirez, M.l. Osendi, Toughening in ceramics containing graphene fillers, Ceram. Inter. 40 (20f4) fff87-fff92.

[3f] E. Zapata−Solvas, D. Gómez−García, A. Domínguez−Rodríguez, Towards physical properties tailoring of carbon nanotubes−reinforced ceramic matrix composites, J. Eur. Ceram. Soc. 3 (20f2) 300f-3020.

[32] N. Garmendia, S. Grandjean, J. Chevalier, L.A. Diaz, R. Torrecillas, l. Obieta, Zirconia−multiwall carbon nanotubes dense nano−composites with anunusual balance between crack and ageing resistance, J. Eur. Ceram. Soc. 3f (20ff) f009-f0f4.

[33] R. Poyato, A. Gallardo−López, F. Gutiérrez−Mora, A. Morales−Rodríguez, A. Muñoz, A. Domínguez−Rodríguez, Effect of high SWNT content on the room temperature mechanical properties of fully dense 3YTZPƒSWNT composites, J. Eur. Ceram. Soc. 34 (20f4) f57f-f579.

[34] A. Duszová, J. Dusza, K. Tomásek, J. Morgiel, G. Blugand, J. Kuebler, Zirconiafcarbon nanofiber composite, Scr. Mater. 58 (2008) 520−523.

[35] J. Dusza, J. Morgiel, A. Duszová, L. Kvetková, M. Nosko, P. Kun, Microstructure and fracture toughness of Si_3N_4+graphene platelet composites, J. Eur. Ceram. Soc. 32 (20f2) 3389−3397.

[36] A. Borrell, R. Torrecillas, V.G. Rocha, A. Fernández, Alumina−carbon nanofibers nanocomposites obtained by spark plasma sintering for proton exchange membrane, Fuel Cells f2 (20f2) 599−605.

[37] J.C. Durand, B. Jacquot, H. Salehi, M. Fages, J. Margerit, F.J.G. Cuisinier, Confocal Raman microscopic analysis of the zirconiaffeldspathic ceramic interface, Dent. Mater. 28 (20f2) 66f-67f.

[38] S. Heiroth, R. Frison, J.L.M. Rupp, T. Lippert, E. Barthazy, E. Müller, K. Conder, A. Wokaun, L.J. Gauckler, Crystallization and grain growth characteristics of yttria−stabilized zirconia thin films grown by pulsed laser deposition, Solid State lonics 191 (20ff) f2-23.

[39] S. Nazarpour, C. López−Gándara, C. Zamani, J.M. Fernández−Sanjuán, J.M. Ramos, A. Cirera, Phase transformation studies on YSZ doped with alumina. Part 2: Yttria Segregation, J. Alloys Compounds 505 (20f0) 534-54f.

[40] L.M. Malard, M.A. Pimenta, G. Dresselhaus, M.S. Dresselhaus, Raman spectroscopy in graphene, Phys. Rep. 437 (2009) 5f-58.

[4f] K.N. Kudin, B. Ozbas, H.C. Schniepp, R.K. Prud'homme, l.A. Aksay, R. Car, Raman spectra of graphite oxide and functionalized graphene sheets, Nano Lett. 8 (2008) 36-4f.

[42] M.S. Dresselhaus, A. Jorio, M. Hofmann, G. Dresselhaus, R. Saito, Perspectives on carbon nanotubes and graphene Raman spectroscopy, Nano Lett. f0 (20f0) 75f-758.

[43] H. Porwal, S. Grasso, M.K. Mani, M.J. Reece, ln situ reduction of graphene oxide nanoplatelet during spark plasma sintering of a silica matrix composite, J. Eur. Ceram. Soc. 34 (20f4) 3357−3364.

[44] C. Ramírez, S.M. Vega−Diaz, A. Morelos−Gomez, F.M. Figueiredo, M. Terrones, M.l. Osendi, M. Belmonte, P. Miranzo. Synthesis of conducting graphenefSi$_3$N$_4$ composites by spark plasma sintering, Carbon 57 (20f3) 425−432.

[45] D. Zhan, Z. Ni, W. Chen, L. Sun, Z. Luo, L. Lai, T. Yu, A.T.S. Wee, Z. Shen, Electronic structure of graphite oxide and thermally reduced graphite oxide, Carbon 49 (20ff) f362-f366.

[46] Y.H. Qin, H.H. Yan, X.S. Zhang, P. Li, C.A. Ma, Effect of carbon nanofibers microstructure on electrocatalytic activities of Pd electrocatalysts for ethanol oxidation in alkaline medium, lnt. J. Hydrogen Energy 35 (20f0) 7667−7674.

[47] P. Delhaes, M. Couzi, M. Trinquecoste, J. Dentzer, H. Hamidou, C. Vix−Guterl, A comparison between Raman spectroscopy and surface characterizations of multiwall carbon nanotubes, Carbon 44 (2006) 3005-30f3.

[48] L. Melk, J.J.R. Rovira, M.L. Antti, M. Anglada, Coefficient of friction and wear resistance of zirconia−MWCNTs composites, Ceram. lnter. 4f (20f5) 459−468.

Figure captions:

Figure f. Variation of zeta potential with pH of alumina colloidal suspension in waterfethanol, CNFs in waterfethanol with and without KD7 and GO in water.

Figure 2. Flow curves of ZA suspensions prepared to solids loadings of 20, 23, 28 and 33 vol.% and different sonication times.

Figure 3. Variation of viscosity with solid volume fraction.

Figure 4. Flow curves of 28 vol.% ZACNF suspensions prepared at different sonication times.

Figure 5. Flow curves of 28 vol.% ZAGO suspensions prepared at different sonication times.

Figure 6. FE−SEM micrographs of fracture surfaces of: a) ZA, b) ZACNF, and c) ZAGO composites obtained by SPS at f500 ºC.

Figure 7. Raman spectra of the GO and CNFs starting powders and ZAGO and ZACNF composites obtained by SPS at different temperatures.

Figure 1

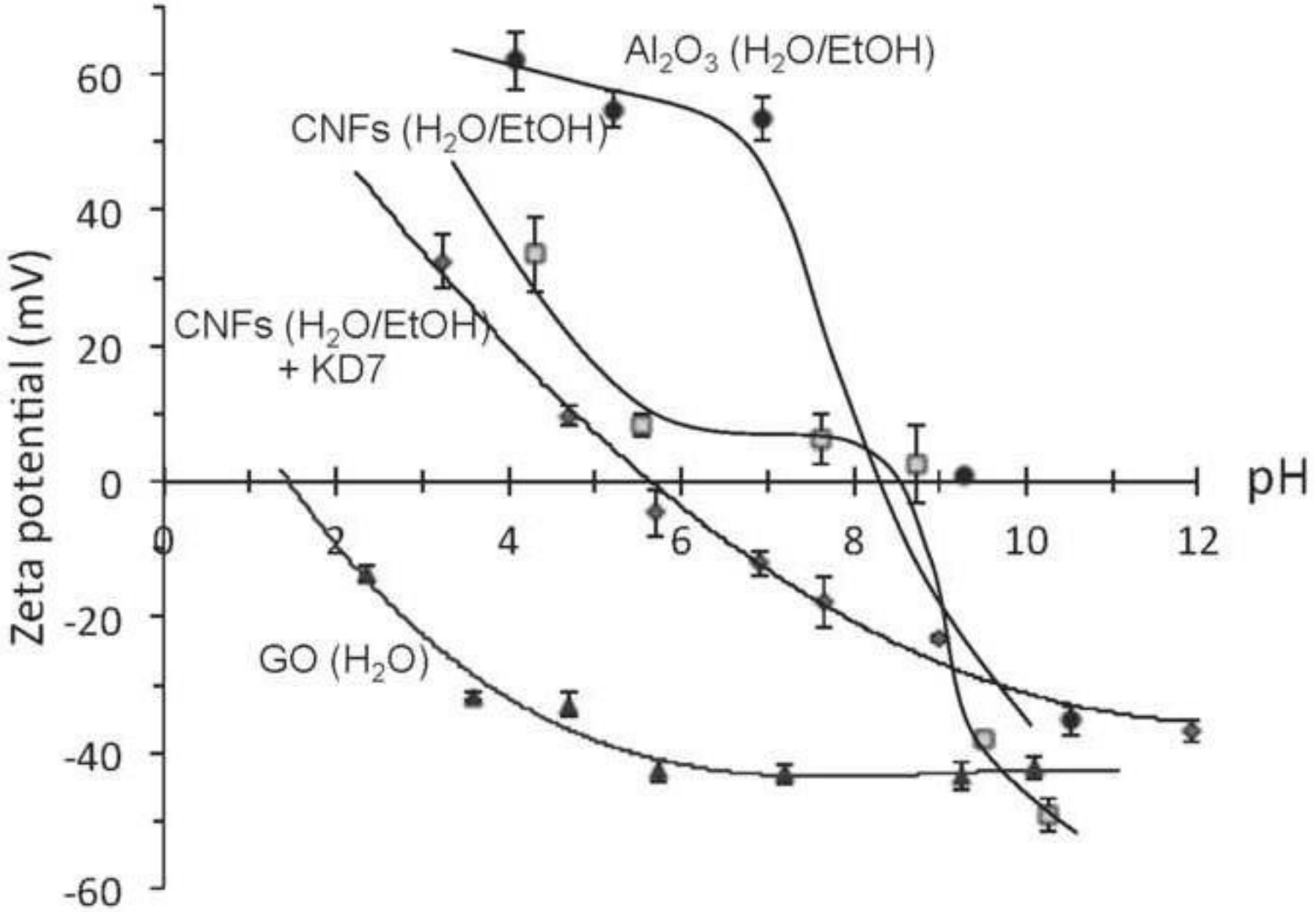

Figure 2

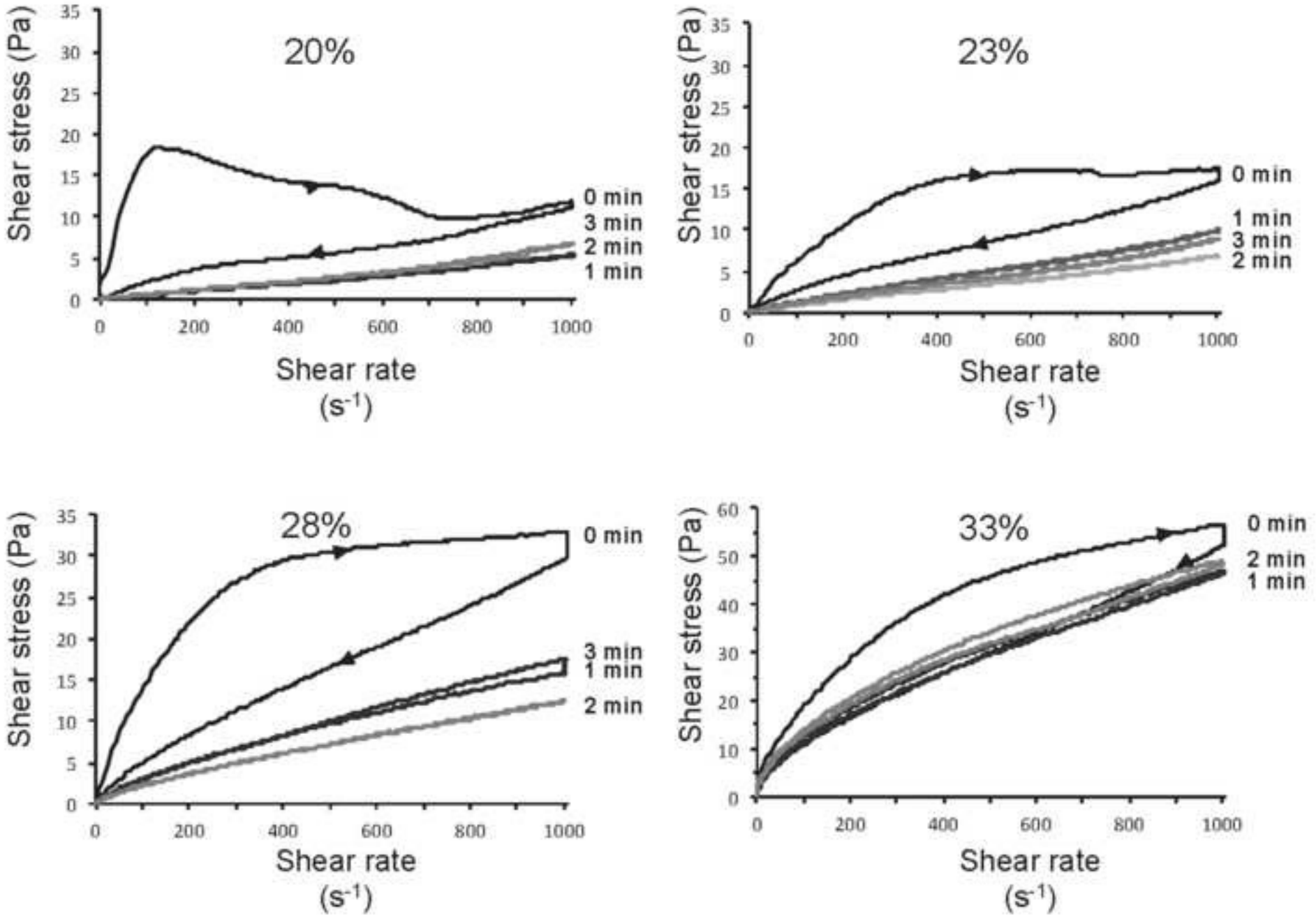

Figure 3

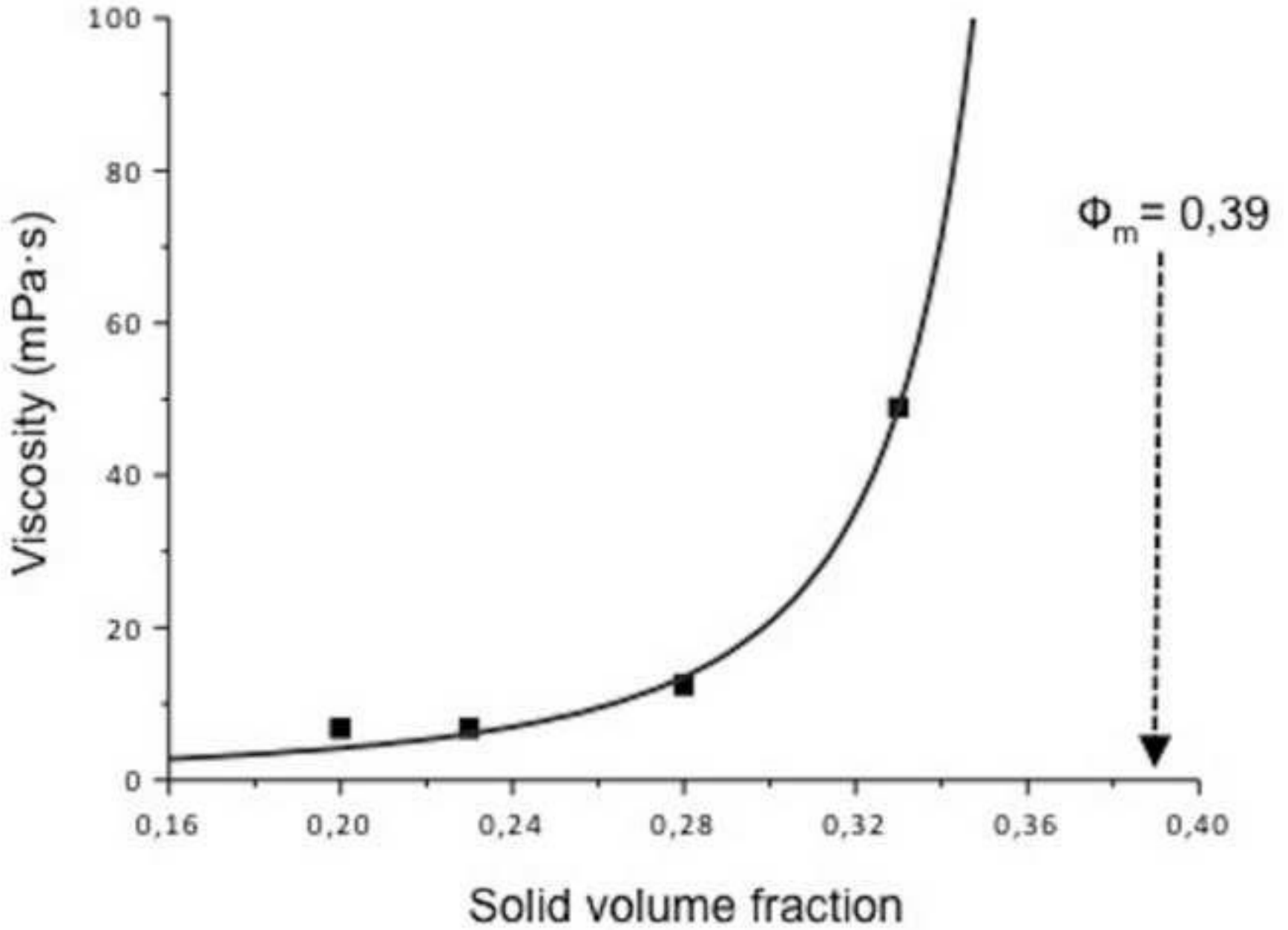

Figure 4

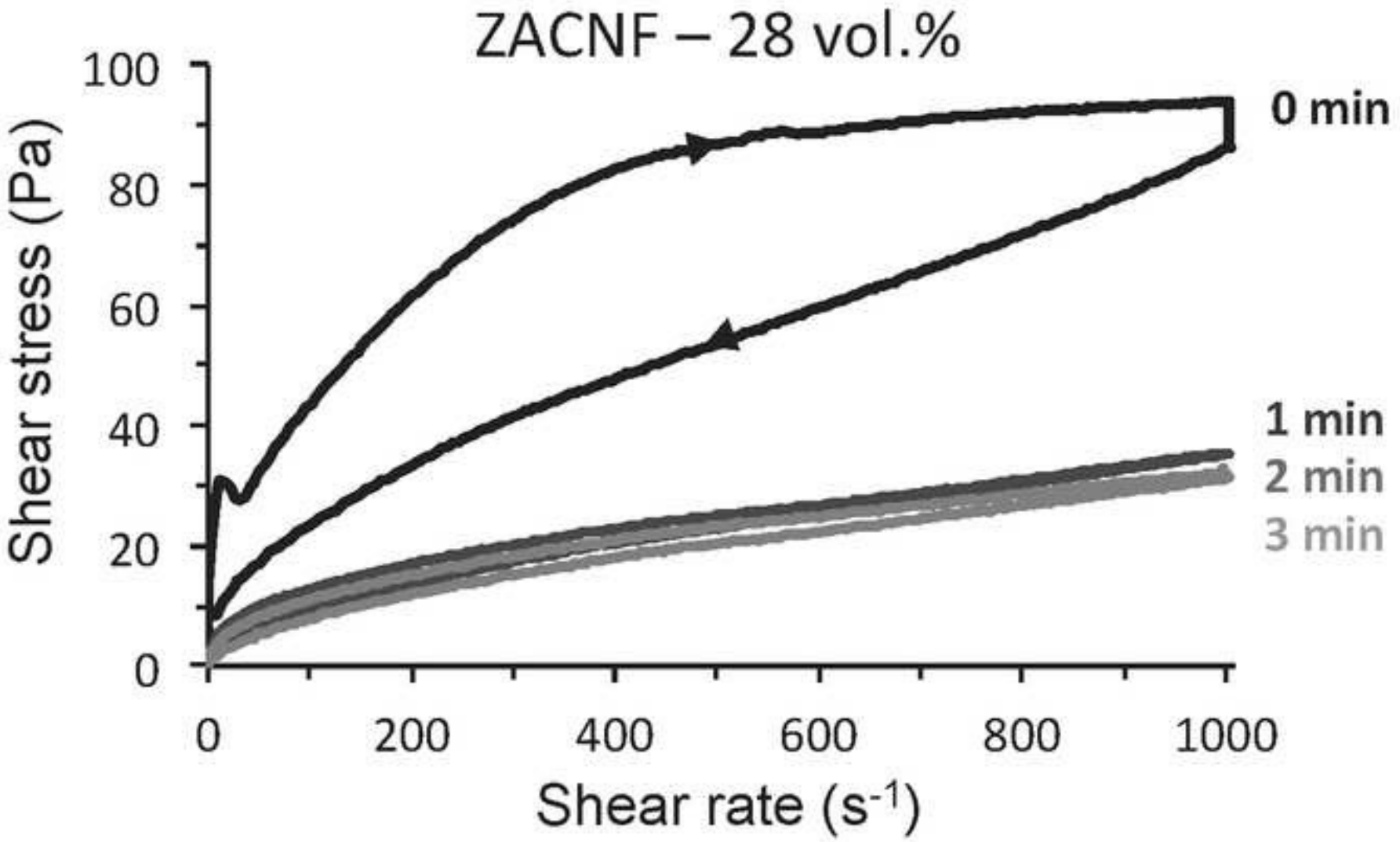

Figure 5

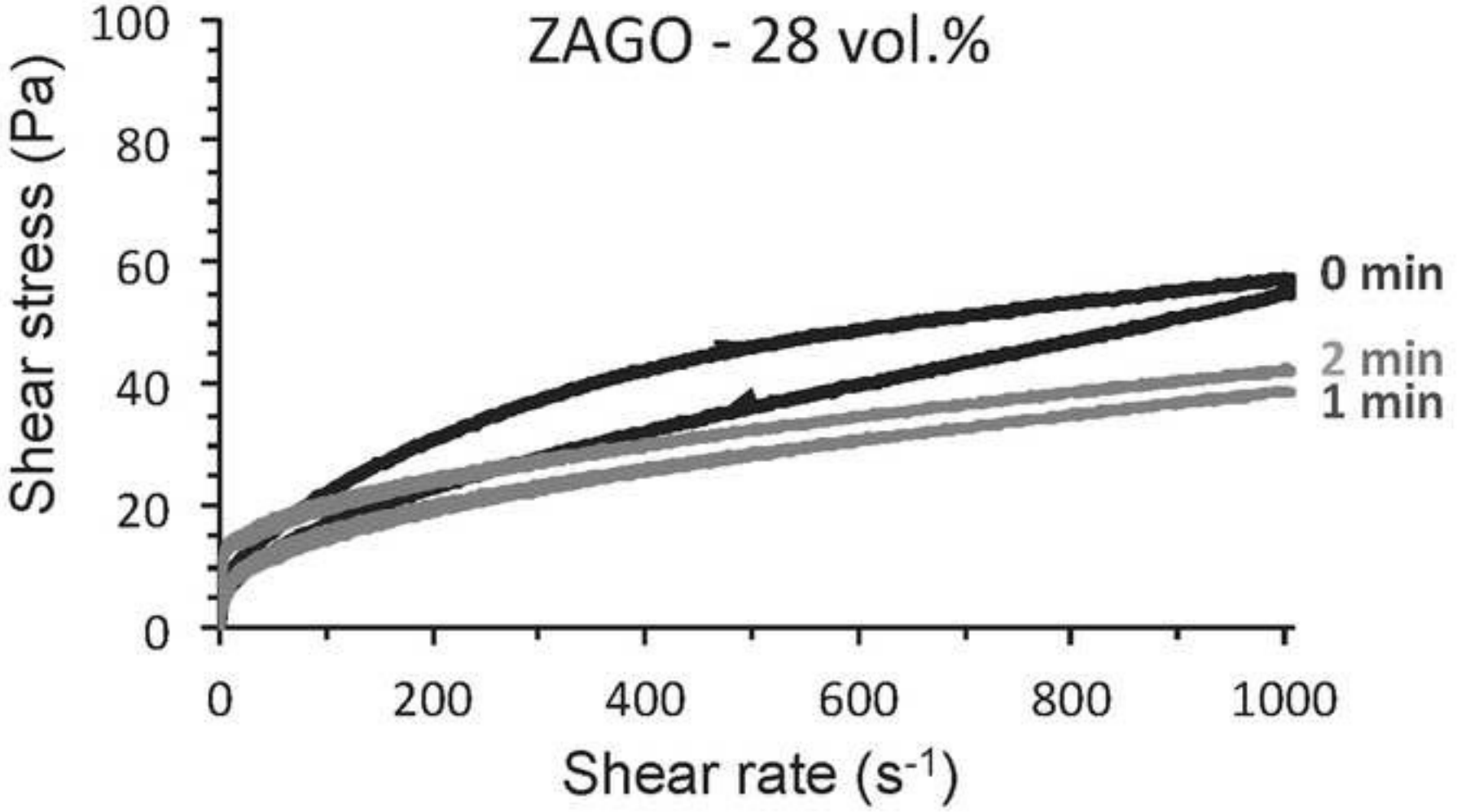

Figure 6

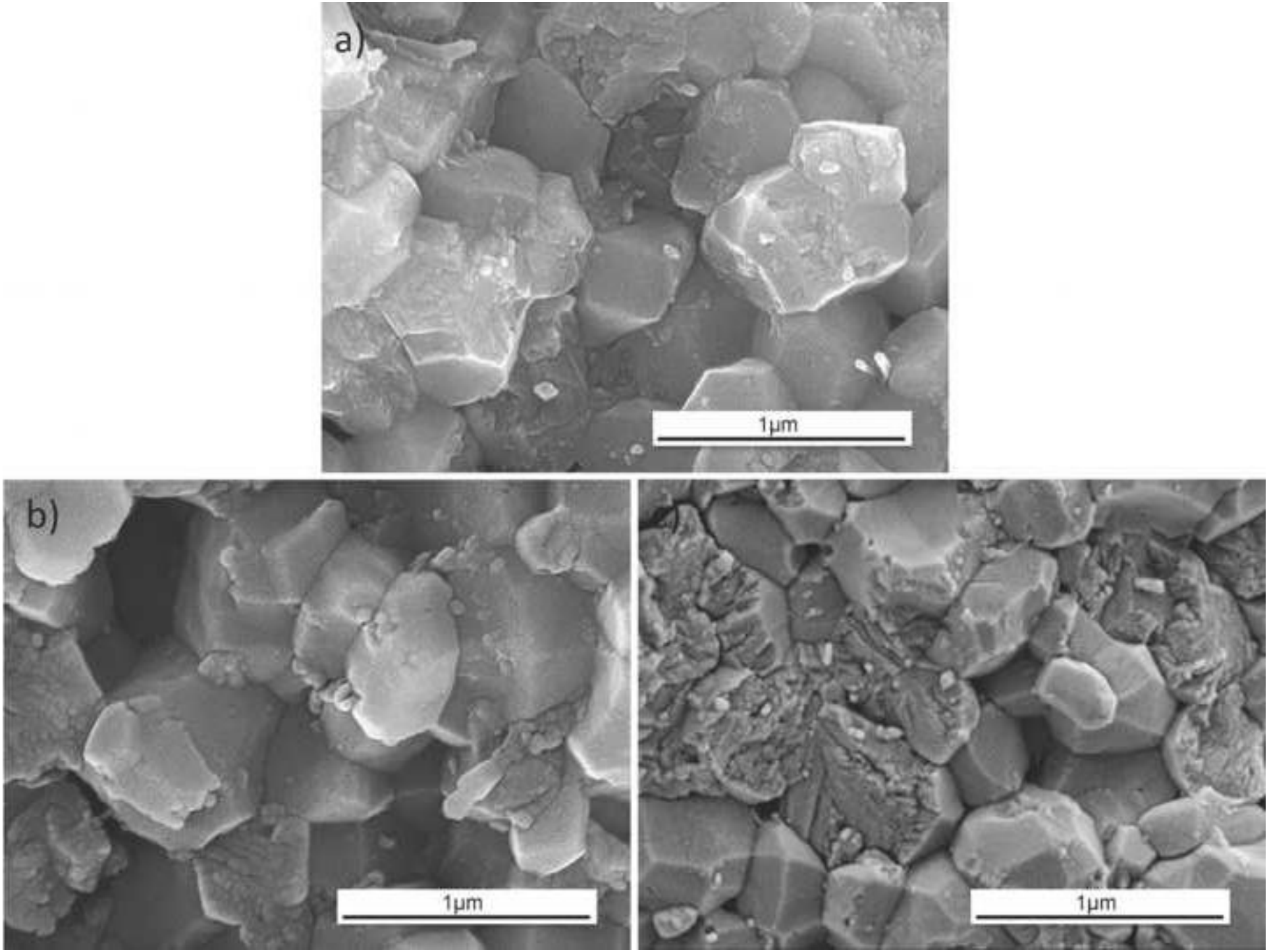

Figure 7

Click here to download high resolution image